Supporting Information

Barash et al. 10.1073/pnas.0908867107

miR-34A up-regulation

Previous global microRNA (miRNA) expression analyses identified a cohort of miRNAs that exhibit p53-dependent up-regulation following DNA damage (1, 2). miR-34a is directly transactivated by p53 and induces apoptosis and cell cycle arrest in the G_1-phase, thereby suppressing tumor cell proliferation and DNA repair (1, 2). We have found up-regulation of miR-34A in 9-month-old $Mdr2^{-/-}$ mice, which, following normalization, was about 8-fold higher than the level of its expression in the controls. This up-regulation of miR-34A in the $Mdr2^{-/-}$ mice supports our conclusion that the DNA damage response pathway is activated in these mice.

SI Materials and Methods

Mice. All experiments were performed in accordance with the guidelines and approval of the Animal Care and Use Committee of the Hebrew University [the Animal Care Unit holds National Institutes of Health (NIH) approval number OPRR-A01-5011 and American Association for the Accreditation of Laboratory Animal Care International accreditation number 1285]. Founders of the FVB.129P2-Abcb4^{tm1Bor} ($Mdr2^{-/-}$; formerly FVB.129P2-Pgy24^{tm1Bor}) and WT FVB/NJ mice were purchased from the Jackson Laboratory. The F1 hybrids produced by breeding of FVB.129P2-Abcb4^{tm1Bor} and FVB/NJ mice were used as age-matched controls.

MRI. Liver MRI scans were acquired on a 4.7-T Biospec spectrometer (Bruker) using a 3.5-cm birdcage coil on mice anesthetized with pentobarbital (30 mg/kg) at baseline and after surgery—on days 2, 4, 6/7, 10, and 14 and once a month thereafter until the age of 12 months (Fig. S1). Liver volumetric follow-up was performed by coronal and axial T_1-weighted spin echo [SE; repetition time (TR)/echo time (TE) = 400/18 ms], and tumorigenesis was assessed using T_2-weighted fast SE (TR/TE = 2,000/40 ms). Volume analysis was performed using Analyze 6.0 (Biomedical Imaging Resource; Mayo Clinic). Liver volume was expressed as a percentage of the preoperative liver volume.

PHx. Thirty-five percent and 70% PHx or sham surgery was performed according to the method of Higgins and Anderson (3) adapted to mice (4) on 3-month-old (inflamed liver), 6-month-old, and 9-month-old (preneoplastic stages) $Mdr2^{-/-}$ mice and age-matched control mice (Fig. S1). At the indicated times, animals were injected with BrdU (Amersham; 10 μL/g body weight i.p.) and killed after 3 h. Livers were rapidly excised, and one part was fixed in formalin for histology; the remaining liver tissue was snap-frozen for RNA analyses or frozen sections.

Immunohistochemistry. Immunohistochemistry was performed on paraffin-embedded sections (5 μm). Slides were deparaffinized in xylene and rehydrated through a series of ethanol washes, incubated in 3% H_2O_2 (3 ml of H_2O_2 in 100 ml of methanol) for 5 min and washed in PBS, subjected to microwave antigen retrieval and washed in PBS, and incubated again in 3% H_2O_2 (3 ml of H_2O_2 in 100 ml of methanol) for 5 min and washed in PBS and then Optimax (Biogenex). We used the following antibodies in blocking solution: mouse antibody to CDC47 (1:100 dilution; Biocare Medical), mouse antibody to γ-H2AX (1:100 dilution, 05-636; Upstate), rabbit antibody to rabbit Chk2-T68 (1:50 dilution; Abcam), mouse antibody to P21 (1:50 dilution, sc-6246; Santa Cruz), and rabbit polyclonal antibody to CDC2 phospho-(Tyr15) (1:50 dilution; Novus Biologicals). Slides were incubated with the antibodies overnight at 4 °C, washed in Optimax, and incubated with the appropriate secondary antibody (Envision$^+$; DAKO) for 30 min at room temperature. Following a PBS wash, signal was developed using AEC substrate (DAKO). For the immunostaining of γ-H2AX and Chk2-T68 antibodies, we incubated the slides with DNase for 12 min at room temperature after the second H_2O_2 treatment. Antigen retrieval was performed using EDTA (pH 8.0) for γ-H2AX, 100 mM glycine (pH 9.0) for CDC47, and 25 mM citrate buffer (pH 6.0) for P21 and Chk2-T68.

BrdU staining was performed using a Cell proliferation kit (Amersham) according to the manufacturer's protocol. We performed TUNEL staining with an in situ Cell Death Detection Kit (Roche Diagnostics) according to the manufacturer's protocol. We stained the nuclei with DAPI. Histology was observed by a professional pathologist. The number of positive cells was counted in 10 randomly selected high-power microscopic fields (400× magnification) for each slide, and the mean value ± SD was determined.

Immunofluorescent Staining. We placed liver specimens in Tissue-Tek optimum cutting-temperature compound, snap-froze them in liquid nitrogen, and stored them at −80 °C. Cryostat sections (10 μm) were produced. Samples were rehydrated with 4% paraformaldehyde (Gadot Ltd, Israel) for 20 min, washed in PBS, and then blocked with 10% donkey serum (10 ml serum in 100 PBS) and 0.2% Triton at room temperature for 45 min. We then incubated samples with anti-53bp1 (Bethyl) for 2.5 h at room temperature and with anti-rabbit FITC at a 1:50 dilution for 1 h at room temperature. Counterstaining was performed using DAPI. For senescence analysis, cryostat sections (5 μm) were freshly cut and samples were fixed in 0.5% glutaraldehyde solution and washed with PBS/$MgCl_2$ (pH 6.0). The slides were then incubated for 24 h at 37 °C in freshly prepared senescence-associated-β-gal staining solution containing 1 mg/mL X-gal (Calbiochem). Postfixation was performed in 4% formalin, and counterstaining was performed with eosin.

Gene Expression Profiling. RNA was isolated from liver samples of 9-month-old $Mdr2^{-/-}$ and control mice obtained on days 0 (the removed lobe), 2, and 6 following PHx (Figs. S1*B* and S3). Total RNA was isolated from frozen liver tissues with TRIzol reagent (Invitrogen) as described by the manufacturer and subjected to genome-scale gene expression profiling using Mouse Genome Array 430A (Affymetrix, Inc.). Array data were normalized by the GCRMA algorithm (5, 6) using R and bioconductor (http://www.bioconductor.org/). Gene and gene ontology annotations were determined for each probe set according to the annotation files published in the Affymetrix web site (www.affymetrix.com). Log_2-normalized expression values, after thresholding and filtering, were submitted to unsupervised cluster analysis using Cluster software (7). A paired *t* test and two-way ANOVA for the factors day and strain were performed using Matlab software (Mathworks, Inc.). The gene expression data discussed in this article were deposited in NCBI's GEO (accession no. GSE14539) and are accessible through the NCBI tracking system (no. 15577663).

Analysis of Overrepresented Functional Categories. The Database for Annotation, Visualization, and Integrated Discovery (DAVID) 2007, a bioinformatics tool provided by the NCBI (http://david.abcc.ncifcrf.gov/), was used to determine functional biological categories. DAVID 2007 utilizes several annotation systems, including gene ontology categories, Protein Information Resource, UniProt (formerly SwissProt) keywords, and pathway maps, to summarize the functional information in a large dataset.

CGH Analysis. Genomic DNA was isolated from nontumorous and HCC tumorous liver tissue samples of 9-month-old Mdr2$^{-/-}$ mice that were subjected to 70% PHx at the age of 6 months (n = 4). Tumor volume was measured by calipers. The samples were frozen immediately after surgery and stored at −80 °C. DNA was extracted using the Wizard Genomic DNA Purification Kit (Promega, USA) according to the manufacturer's protocol. Quantitation of the genomic DNA samples was performed using the Qubit fluorometer and the Quant-iT dsDNA BR Assay Kit (Invitrogen). CGH analysis was carried out at Miltenyi Biotec GmbH in Germany. A total of 1.5 μg of each DNA sample was used for restriction enzyme digestion with the restriction enzymes *Alu*I and *Rsa*I. The digested DNA was utilized as a template for a genomic DNA labeling reaction using the Genomic DNA Labeling Kit PLUS (Agilent Technologies) according to the manufacturer's protocol. The hybridization procedure was performed according to the Agilent Oligonucleotide Array-Based CGH for Genomic DNA Analysis protocol V5.0 using the Agilent Oligo aCGH Hybridization Kit (Agilent Technologies). The corresponding Cy3- and Cy5-labeled DNA was combined and hybridized at 65 °C for 24 h to an Agilent Mouse Genome CGH Microarray 4 × 44K, using Agilent's recommended hybridization chamber and oven. Fluorescence signals of the hybridized Agilent Mouse Genome CGH Microarrays were detected using Agilent's DNA microarray scanner (Agilent Technologies). Agilent Feature Extraction Software was used to read out and process the microarray image files. Further analysis and visualization of the hybridization results were performed with Agilent CGH Analytics software (V3.5). Here, the following aberration filter settings have been used: (*i*) minimum number of probes present in an aberrant region = 2; (*ii*) minimum absolute average $\log_2$ ratio for region = 0.4, corresponding to a fold change of 1.32; and (*iii*) statistical analysis of aberrant regions based on the aberrations detection method ADM-2.

Statistical Analysis. Results are expressed as means ± SD. Differences between groups were identified by the unpaired Student's t test, Mann–Whitney exact test, or Kruskal–Wallis test. A hypergeometrical test was performed to assess over-representation of the chromosomal instability (CIN) signature (70 CIN), as published by Carter et al. (8). A P value less than 0.05 was considered to be statistically significant. The Mann–Whitney test was performed using GraphPad InStat version 3.06 for Windows.

1. Tarasov V, et al. (2007) Differential regulation of microRNAs by p53 revealed by massively parallel sequencing: miR-34a is a p53 target that induces apoptosis and G1-arrest. *Cell Cycle* 6:1586–1593.
2. Chang TC, et al. (2007) Transactivation of miR-34a by p53 broadly influences gene expression and promotes apoptosis. *Mol Cell* 26:745–752.
3. Higgins GM, Anderson RM (1931) Experimental pathology of the liver. I. Restoration of the liver of the white rat following partial surgical removal. *Arch Pathol* 12: 186–202.
4. Greene AK, Puder M (2003) Partial hepatectomy in the mouse: Technique and perioperative management. *J Invest Surg* 16:99–102.
5. Gentleman RC, et al. (2004) Bioconductor: Open software development for computational biology and bioinformatics. *Genome Biol* 5:R80.
6. Wu ZJ, Irizarry RA, Gentleman R, Martinez-Murillo F, Spencer F (2004) A model-based background adjustment for oligonucleotide expression arrays. *J Am Stat Assoc* 99: 909–917.
7. Eisen MB, Spellman PT, Brown PO, Botstein D (1998) Cluster analysis and display of genome-wide expression patterns. *Proc Natl Acad Sci USA* 95:14863–14868.
8. Carter SL, Eklund AC, Kohane IS, Harris LN, Szallasi Z (2006) A signature of chromosomal instability inferred from gene expression profiles predicts clinical outcome in multiple human cancers. *Nat Genet* 38:1043–1048.

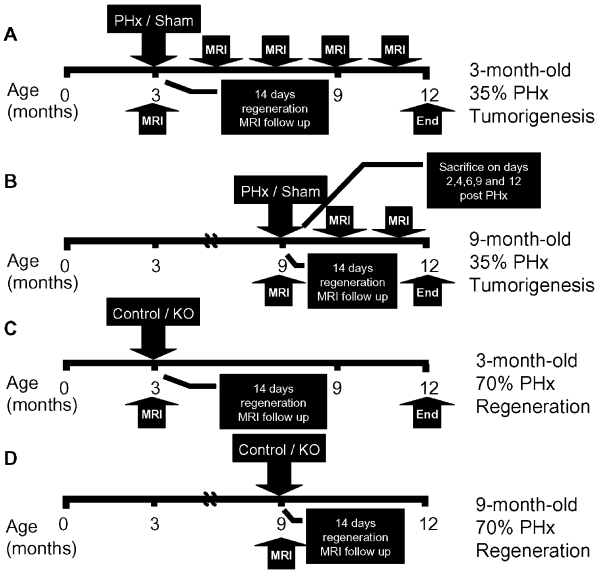

Fig. S1. Experimental schedule. We have performed 35% (*A* and *B*) or 70% (*C* and *D*) PHx on 3-month-old (*A* and *C*) and 9-month-old (*B* and *D*) mice. We compared tumorigenesis development in Mdr2$^{-/-}$ mice that have gone through sham or PHx surgery in 3-month-old (*A*) and 9-month-old (*B*) mice. We performed MRI scans before surgery and followed these mice by MRI once a month until the age of 1 year. At this age, they were scanned and killed. We compared regeneration in Mdr2$^{+/-}$ or Mdr2$^{+/+}$ mice to that in Mdr2$^{-/-}$ mice in 3-month-old (*C*) and 9-month-old (*D*) mice. We performed MRI scans before surgery and followed these mice by MRI on days 2, 4, 6, 10, and 14 following PHx. (*B*) In addition, we killed mice on days 2, 4, 6, 9, and 12 following PHx and excised their livers for histology and RNA production. The resected lobes represented day 0.

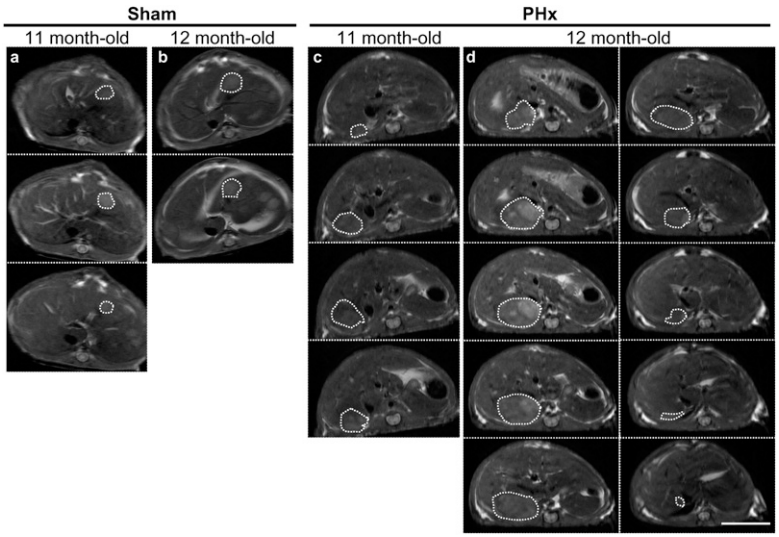

Fig. S2. Accelerated tumorigenesis. Representative T_2-weighted axial MRI scans of two mice at two different time points, 11 months (*A* and *C*) and 12 months (*B* and *D*), that underwent sham surgery (*A* and *B*) or PHx (*C* and *D*) at the age of 9 months. The figures illustrate the same tumor in each mouse as they enlarge in time (*A* to *B* compared with *C* to *D*). White dotted lines encircle tumors. (Scale bar: 1 cm.)

A

	Control (+/-)	KO (-/-)
Pre	3	6
Day 2	3	3
Day 6	3	3

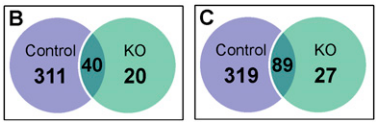

Fig. S3. Gene expression analysis. (*A*) Table describes the number of arrays performed for each genotype, $Mdr2^{+/-}$ (control) or $Mdr2^{-/-}$ mice (KO), at three different time points: the resected lobe (day 0), and days 2 and 6 following PHx. Each array represents one mouse. The resected lobe is from the same mice that were killed on day 2 or 6 following PHx. (*B* and *C*) Venn diagram representing up-regulated genes (>2-fold) on day 2 (*B*) or 6 (*B*) following PHx compared with the resected lobe (day 0).

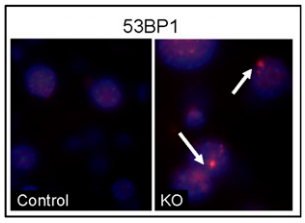

Fig. S4. We confirmed the presence of DNA damage in the livers of $Mdr2^{-/-}$ mice (KO) using immunostaining for nuclear foci of the protein 53BP1, which accumulates at DSB sites. Representative stained liver sections of 9-month-old control and $Mdr2^{-/-}$ (KO) mice obtained before PHx (DAPI, blue; 53BP1, red).

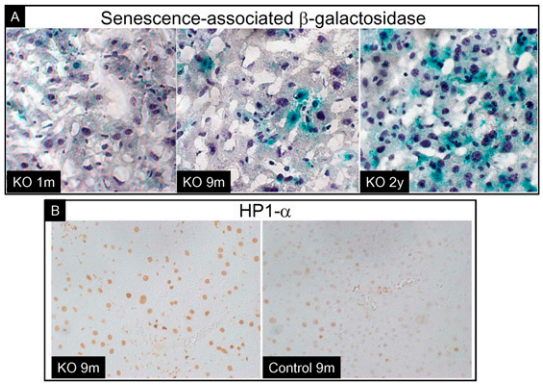

Fig. S5. Markers for senescence. (*A*) Senescence-associated β-galactosidase expression in livers of Mdr2$^{-/-}$ mice (KO) at the age of 1 month (*Left*), 9 months (*Center*), and 2 years (*Right*). (*B*) Immunofluorescence using anti-HP1-α staining of 9-month-old Mdr2$^{-/-}$ (KO) and control mice, which indicates senescence-associated heterochromatin foci.

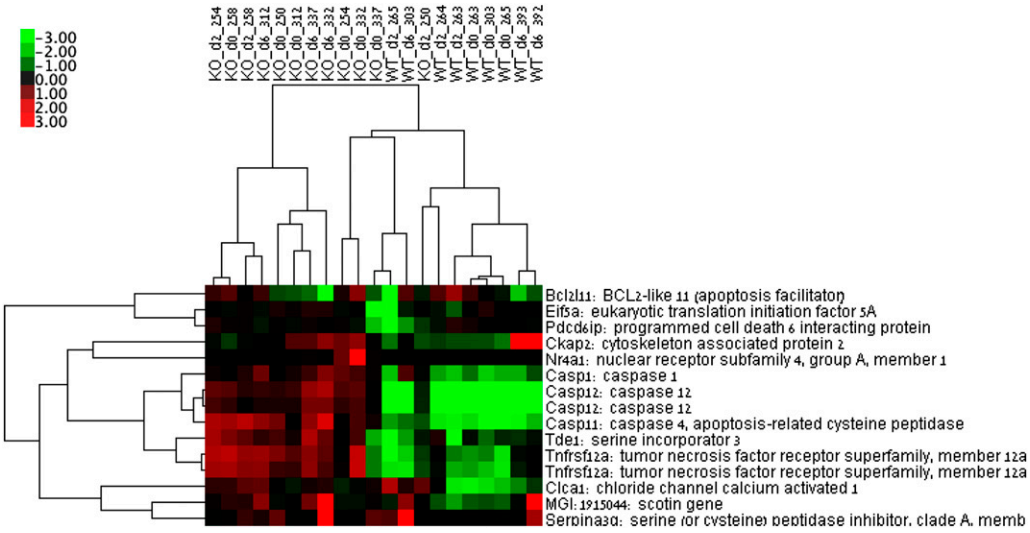

Fig. S6. Proapoptotic genes. A cluster analysis of the expression of proapoptotic genes comparing Mdr2$^{+/-}$ (WT) or Mdr2$^{-/-}$ mice (KO) from the resected lobe on day 0 (d0) and days 2 (d2) and 6 (d6) following PHx. Columns represent individual samples, and rows represent each gene. Each cell in the matrix represents the expression level of a gene feature in an individual sample. Red and green in cells reflect high and low expression levels, respectively, as indicated in the scale bar (log_2-transformed scale).

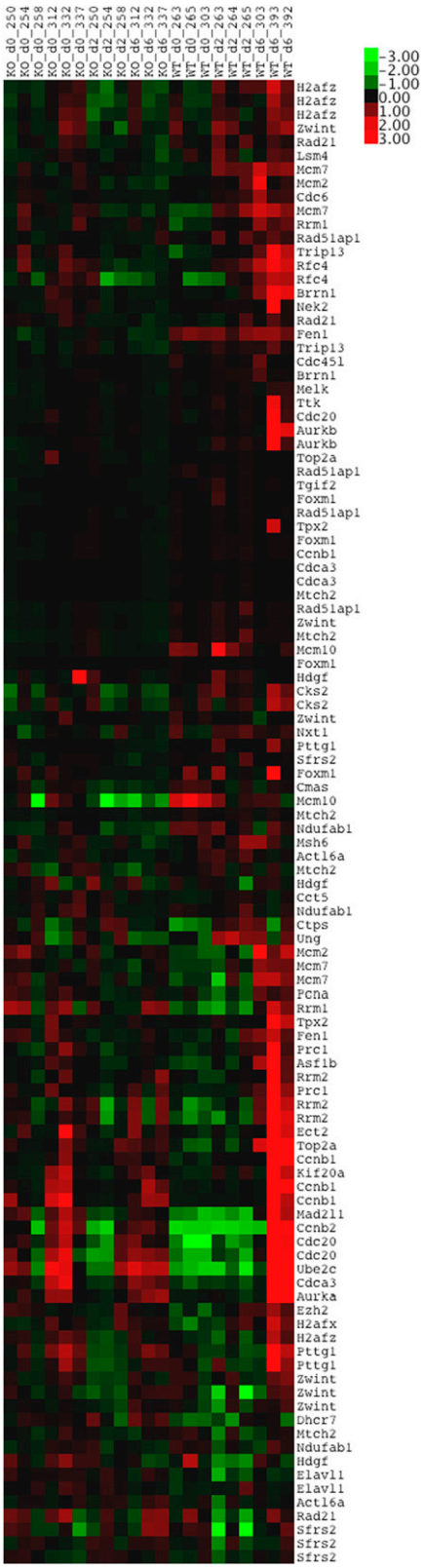

Fig. S7. Chromosomal instability signature genes. A cluster analysis of the expression of chromosomal instability signature genes as described by Carter et al. [Carter SL, Eklund AC, Kohane IS, Harris LN, Szallasi Z (2006) A signature of chromosomal instability inferred from gene expression profiles predicts clinical outcome in multiple human cancers. *Nat Genet* 38:1043–1048] comparing $Mdr2^{+/-}$ (WT) or $Mdr2^{-/-}$ mice (KO) from the resected lobe on day 0 (d0) and days 2 (d2) and 6 (d6) following PHx. Columns represent individual samples, and rows represent each gene. Each cell in the matrix represents the expression level of a gene feature in an individual sample. Red and green in cells reflect high and low expression levels, respectively, as indicated in the scale bar (log_2-transformed scale). Genes involved in chromosomal instability are up-regulated in the control mice on day 6 following PHx. The $Mdr2^{-/-}$ mice show negative enrichment of these genes on day 6 ($P < 0.05$) compared with control mice.

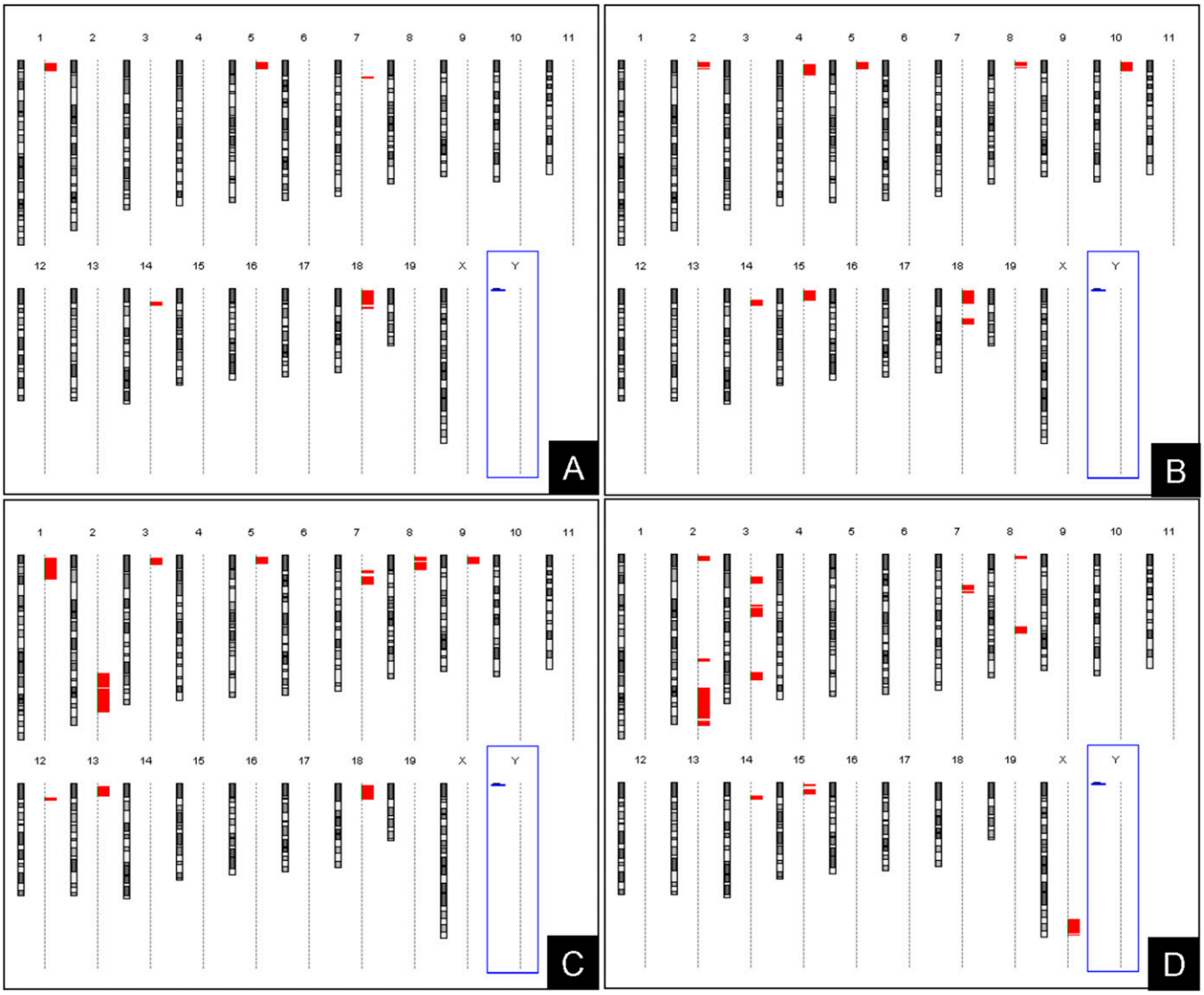

Fig. S8. CGH analysis results. Chromosomal locations of copy number changes in four HCC tumor samples from 9-month-old Mdr2$^{-/-}$ mice that underwent PHx at the age of 6 months, using Agilent 44K CGH arrays. CGH analytics view presents the DNA copy number profile across all chromosomes. Detected aberrations are marked with red boxes for amplifications. The CGH results demonstrated prolonged amplifications in all four tumors, with no detectable deletion.

A

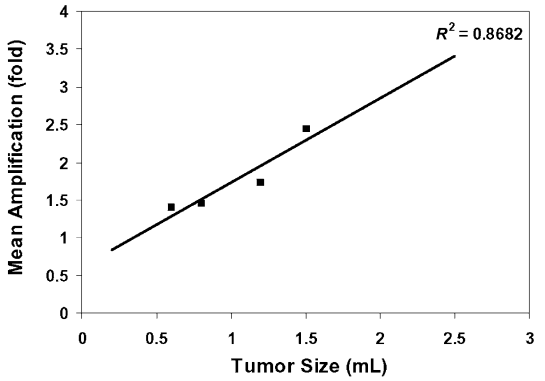

B

Site in mice	Fold enhancement In Mdr2$^{-/-}$ mice	Syntenie Fragile Site in Humans
5qA1	1.3-3.1	7q11
8qA1	1.6-2.2	19p13

Fig. S9. (*A*) Correlation between HCC tumor size (mL) and the mean amplification-fold of the amplified regions in four HCC tumor samples from 9-month-old Mdr2$^{-/-}$ mice that underwent PHx at the age of 6 months. (*B*) Two of the common amplified regions in the HCC tumors are syntenic to chromosomal regions that are frequently amplified in human HCC.